

Theoretical design of thermal spin molecular logic gates by using a combinational molecular junction

Yi Guo(郭逸), Peng Zhao(赵朋), and Gang Chen(陈刚)
Citation: Chin. Phys. B, 2022, 31 (**4**): 047202. DOI: 10.1088/1674-1056/ac3a5f
Journal homepage: http://cpb.iphy.ac.cn; http://iopscience.iop.org/cpb

What follows is a list of articles you may be interested in

Separating spins by dwell time of electrons across parallel double *δ*-magnetic-barrier nanostructure applied by bias

Sai-Yan Chen(陈赛艳), Mao-Wang Lu(卢卯旺), and Xue-Li Cao(曹雪丽)
Chin. Phys. B, 2022, 31 (**1**): 017201. DOI: 10.1088/1674-1056/abeb09

Different noncollinear magnetizations on two edges of zigzag graphene nanoribbons

Yang Xiao(肖杨), Qiaoli Ye(叶巧利), Jintao Liang(梁锦涛), Xiaohong Yan(颜晓红), and Ying Zhang(张影)
Chin. Phys. B, 2020, 29 (**12**): 127201. DOI: 10.1088/1674-1056/abc0e4

Theoretical design of single-molecule NOR and XNOR logic gates by using transition metal dibenzotetraaza[14]annulenes

Zi-Qun Wang(王子群), Fei Tang(唐菲), Mi-Mi Dong(董密密), Ming-Lang Wang(王明郎), Gui-Chao Hu(胡贵超), Jian-Cai Leng(冷建材), Chuan-Kui Wang(王传奎), Guang-Ping Zhang(张广平)
Chin. Phys. B, 2020, 29 (**6**): 067202. DOI: 10.1088/1674-1056/ab84cf

Electrically tunable spin diode effect in a tunneling junction of quantum dot

Xukai Peng(彭许凯), Zhengzhong Zhang(张正中)
Chin. Phys. B, 2019, 28 (**12**): 127202. DOI: 10.1088/1674-1056/ab53d0

Magnetization-direction-dependent inverse spin Hall effect observed in IrMn/NiFe/Cu/YIG multilayer structure

Runrun Hao(郝润润), Ruxue Zang(臧如雪), Tie Zhou(周铁), Shishou Kang(康仕寿), Shishen Yan(颜世申), Guolei Liu(刘国磊), Guangbing Han(韩广兵), Shuyun Yu(于淑云), Liangmo Mei(梅良模)
Chin. Phys. B, 2019, 28 (**3**): 037202. DOI: 10.1088/1674-1056/28/3/037202

Theoretical design of thermal spin molecular logic gates by using a combinational molecular junction

Yi Guo(郭逸)[1], Peng Zhao(赵朋)[1,†], and Gang Chen(陈刚)[2]

[1] *School of Physics and Technology, University of Jinan, Jinan* 250022, *China*
[2] *School of Physics and Electronics, Shandong Normal University, Jinan* 250358, *China*

(Received 21 August 2021; revised manuscript received 31 October 2021; accepted manuscript online 17 November 2021)

Based on the density functional theory combined with the nonequilibrium Green function methodology, we have studied the thermally-driven spin-dependent transport properties of a combinational molecular junction consisting of a planar four-coordinate Fe molecule and a 15,16-dinitrile dihydropyrene/cyclophanediene molecule, with single-walled carbon nanotube bridge and electrode. Our results show that the magnetic field and light can effectively regulate the thermally-driven spin-dependent currents. Perfect thermal spin-filtering effect and good thermal switching effect are realized. The results are explained by the Fermi–Dirac distribution function, the spin-resolved transmission spectra, the spatial distribution of molecular projected self-consistent Hamiltonian orbitals, and the spin-resolved current spectra. On the basis of these thermally-driven spin-dependent transport properties, we have further designed three basic thermal spin molecular AND, OR, and NOT gates.

Keywords: thermal molecular logic gate, thermally-driven spin-dependent transport, combinational molecular junction, nonequilibrium Green's function

PACS: 72.25.–b, 85.65.+h, 85.75.–d **DOI:** 10.1088/1674-1056/ac3a5f

1. Introduction

Digital electronic devices are ubiquitous in today's information world. Meanwhile, logic gates are basic building blocks in any modern digital electronic devices. They are devices having one or more than one input and only one output. And the input and the output satisfy a certain logical relationship. Among different kinds of logic gates, the AND, OR and NOT gates are three most essential and elementary logic gates. The AND gate is a logical multiplication device, which only yields an output logic 1 when all of its inputs are logic 1. In Boolean algebra terms the output of an AND gate will be true only when all of its inputs are true. The OR gate is a logical addition device, whose output is logic 1 once any of its inputs are logic 1. In Boolean algebra terms the output of an OR gate will be true once any of its inputs are true. The NOT gate is simply a single input inverter that changes the input of a logic 1 to an output of logic 0 and vice versa. In Boolean algebra terms the output of a NOT gate will be false when its input is true.

In recent years, the design and manufacturing of spin molecular devices being able to perform specific logical functions has attracted ever-increasing attention owing to the rapid development of molecular spintronics.[1–4] In these so-called spin molecular logic gates, magnetic molecular materials can switch among different states under the action of one or more input signals, and such transition leads to a single logical output signal. Evidently, selection of appropriate magnetic molecular materials becomes a key factor to construct spin molecular logic gates. So far, many research groups have paid intensive attention to finding the suitable magnetic molecular materials. For example, taking the magnetic field in different directions as input signals and the produced spin-polarized current or total current as output signal, different research groups proposed zigzag graphene nanoribbon-, zigzag silicene nanoribbon- and Mn-phthalocyanie nanoribbon-based spin molecular AND, OR and NOT gates in the early studies.[5–8] Recently, we also conceived and designed planar four-coordinate Fe (PFCF) molecule-based spin molecular AND, OR, NOT gates, etc.[9] Nevertheless, since the proposed PFCF-based spin molecular gates are very tiny, it is difficult to modulate experimentally the direction of external magnetic field in an adjacent Fe atom region at the moment. Very recently, with an attempt to settle this problem, we have further proposed a novel combinational molecular junction (CMJ), which contains a PFCF molecule and a photochromic molecule (15,16-dinitrile dihydropyrene (DDP)/cyclophanediene (CPD)) linked together in series by a finite single-walled armchair carbon nanotube (SWACNT) bridge.[10] Here, the photochromic molecule is respectively in the DDP/CPD form with rapid response time upon the ultraviolet (UV)/visible (VIS) photo-excitation.[11–13] By utilizing the magnetic field in different directions, the light of different wavelengths as input signals and the produced spin-polarized current or total current as an output signal, the spin molecular AND, OR and NOT gates are realized.[10]

In the meantime, with the continuous miniaturization

†Corresponding author. E-mail: ss_zhaop@ujn.edu.cn

© 2022 Chinese Physical Society and IOP Publishing Ltd

of the electronic devices, the problems resulting from the waste heat become more and more serious. Fortunately, spin caloritronics provides a favorable approach to convert untapped waste heat to electricity,[14–16] which increases the energy utilizing efficiency to a large extent. In the present work, we further investigate the thermally-driven spin-dependent transport properties of the PFCF+DDP/CPD-based CMJ. The results demonstrate that the magnetic field and light can effectively regulate the thermally-driven spin-dependent currents. And with that, we can design three elementary thermal spin molecular AND, OR and NOT gates. In the following parts of this article, theoretical model and computational details are given in Section 2. Numerical results and discussion are presented in Section 3. Finally, a conclusion is given in Section 4.

2. Theoretical model and computational details

The studied PFCF+DDP/CPD-based CMJ is schematically depicted in Fig. 1, consisting of the central scattering region (CSR), the hot semi-infinite left and the cold semi-infinite right electrodes (LE and RE, marked by red and green rectangles, respectively). Nonmagnetic metallic (4,4) SWACNTs are adopted as electrodes due to their high electrical conductivity. The CSR includes a PFCF molecule and a DDP/CPD molecule linked in series by a finite (4,4) SWACNT bridge, as well as

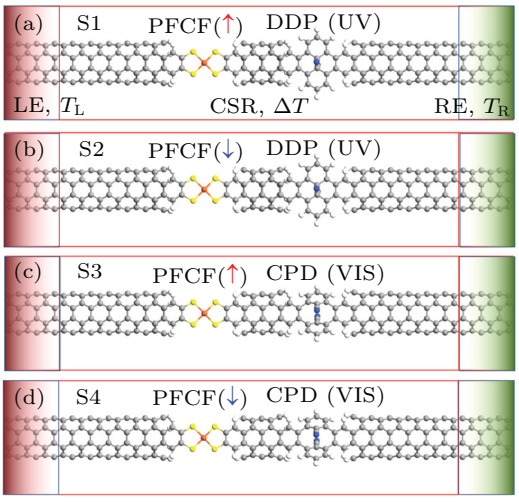


Fig. 1. Schematic of the studied PFCF+DDP/CPD-based combinational molecular junction (CMJ) consisting of a PFCF molecule and a DDP/CPD molecule linked in series by a finite (4,4) SWACNT bridge sandwiched between two (4,4) SWACNT electrodes. The orange, yellow, gray, white and blue spheres stand for the Fe, S, C, H and N atoms, respectively. The CMJ is divided into three regions in simulations: the central scattering region (CSR), the hot semi-infinite left electrode (LE), and the cold semi-infinite right electrode (RE). By tuning the direction of magnetic field (↑= up and ↓= down) and the wavelength of light (UV = ultraviolet and VIS = visible), the CMJ can interconvert among four states, (a) state 1 (S1: the direction of magnetic field is ↑ and the light is UV), (b) state 2 (S2: the direction of magnetic field is ↓ and the light is UV), (c) state 3 (S3: the direction of magnetic field is ↑ and the light is VIS), and (d) state 4 (S4: the direction of magnetic field is ↓ and the light is VIS). A temperature gradient is applied along the CMJ from left to right. T_L and T_R represent the temperature of LE and RE ($T_L > T_R$), respectively, while ΔT indicates the temperature difference between them.

portions of two electrodes to screen out the effect of molecular kernels on bulk electrodes. All the dangling bonds at the open ends of SWACNT electrode and bridge are saturated by H atoms. A thickness of 16 Å in the vacuum interlayer is used in the non-periodic direction to isolate the CMJ from its periodic images. As shown in Figs. 1(a)–1(d), the PFCF+DDP/CPD-based CMJ can interconvert among four states under the action of magnetic field and light, referred to as S1, S2, S3 and S4 in sequence. To be specific, in S1 state (see Fig. 1(a)), the direction of magnetic field is up (↑) and the light is UV. Compared with S1 state, the direction of magnetic field in S2 is changed to down (↓) while the light is still UV (see Fig. 1(b)). In S3 state (see Fig. 1(c)), the direction of magnetic field is ↑ and the light is VIS. Compared with S3 state, the magnetic field is changed to ↓ while the light is still VIS (see Fig. 1(d)). Before the spin caloritronic transport calculations, the CSR is fully relaxed until the force tolerance of 0.02 eV/Å is met.

All the calculation are carried out by using the density functional theory (DFT) combined with the non-equilibrium Green function (NEGF) methodology, as implemented in the software package of Atomistix Toolkit (ATK).[17–20] This methodology has been widely adopted to deal with the thermally-driven spin-dependent transport properties in molecular junctions.[21–25] The exchange–correlation energy is treated by the spin generalized gradient approximation (SGGA) with the Perdew–Burke–Ernzerhof (PBE) functional.[26] To ensure the computational accuracy, the wavefunction of valence electrons are expanded by the double-ζ plus polarization (DZP) basis set, while the electron-ion interactions are modeled by the Troullier–Martins norm-conserving pseudopotentials.[27] Also, a k-mesh of $1 \times 1 \times 21$ and $1 \times 1 \times 100$ according to the Monkhorst–Pack scheme[28] is employed in the geometry relaxation and thermally-driven spin-dependent transport calculations, respectively, while the cutoff energy for the electrostatic potentials is set to be 200 Ry. A temperature gradient is applied along the CMJ from the left to the right, and then the thermally-driven spin-polarized current flowing through the CMJ under the temperature difference ($\Delta T = T_L - T_R$) between the temperature of LE (T_L) and the temperature of RE (T_R) can be obtained via the Landauer–Büttiker formula[29]

$$I_\sigma = \frac{e}{h}\int_{-\infty}^{+\infty} T_\sigma(E)[f_L(E,T_L) - f_L(E,T_R)]\,\mathrm{d}E, \qquad (1)$$

where $T_\sigma(E)$ is the spin-resolved transmission function with the spin index σ (up or down indicating spin-up and spin-down), and $f_{L(R)}$ is the Fermi–Dirac distribution function of electrons in LE (RE). Here, E is the carrier (electron or hole) energy. Moreover, a positive (negative) current represents the flow of current from the LE (RE) to RE (LE). Meantime, we must point out that in ATK code one can set the initial relative spin for every atom in a molecular junction to simulate

the effect of the magnetic field. To be specific, when the initial relative spin of iron atom in the PFCF molecule is set to be 1, it indicates the magnetic field is up; whereas, when the initial relative spin of iron atom in the PFCF molecule is set to be -1, it indicates the magnetic field is down. Then, after a self-consistent DFT+NEGF calculation, one can get the converged spin densities. Furthermore, we calculate the transport properties of CMJ with closed-ring state DDP and open-ring state CPD, respectively, to simulate the cases under UV or VIS action. This method has been widely adopted to study the photochromic molecule-based photoswitches.[30–32]

3. Results and discussion

3.1. Thermally-driven spin transport properties

Figures 2(a)–2(d) present the thermally-driven spin-dependent currents as a function of ΔT with $T_{\rm L} = 300$ K for the CMJ in S1, S2, S3 and S4 states, respectively. The cases with $T_{\rm L} = 350$ and 400 K are also tested, which give similar results. It can be seen clearly from Figs. 2(a)–2(d), the magnetic field and light modulations have significant effects on the thermally-driven currents. In S1 state as shown in Fig. 2(a), obvious negative spin-up current ($I_{\rm up}$) can go through the CMJ, while the spin-down current ($I_{\rm dn}$) is forbidden. On the contrary, in S2 state as shown in Fig. 2(b), the $I_{\rm up}$ is blocked, and obvious negative $I_{\rm dn}$ can pass through the CMJ due to the reversal in the direction of magnetic field. Clearly, only one spin channel is open while the other one is closed in S1 and S2 states, giving rise to a significant thermal spin filtering effect. Unlike S1 and S2 states, in S3 and S4 states as shown in Figs. 2(c) and 2(d), both two channels are shut down, and there is almost no observable $I_{\rm up}$ and $I_{\rm dn}$ flowing through the CMJ due to the photochromic molecule is in the CPD form under the action of VIS light regardless of the direction of the magnetic field. This will undoubtedly cause the total thermally-driven current ($I_{\rm sum} = I_{\rm up} + I_{\rm dn}$) in S1/S2 state to be much larger than that in S3/S4 state. And a good thermal switching effect can be achieved when the CMJ converts between S1 and S3 (S2 and S4) states upon photo-excitation.

The observed thermal spin-filtering and thermal switching effects can be quantified by two parameters, namely, the spin-filtering efficiency (SFE) and switching ratio (SR). The former is the relative ratio of current with a particular spin index over the other and defined as SFE $= [(I_{\rm up} - I_{\rm dn})/(I_{\rm up} + I_{\rm dn})] \times 100\%$. The latter is the absolute ratio of total current between different states and defined as SR $= (I_{\rm sum}$ in S1$)/(I_{\rm sum}$ in S3$) \times 100\%$ and $(I_{\rm sum}$ in S2$)/(I_{\rm sum}$ in S4$) \times 100\%$, respectively. Figure 3(a) plots the SFE as a function of ΔT for the CMJ in S1 and S2 states. It is evident that both S1 and S2 states exhibit perfect spin-filtering performance with the SFEs approaching to $\pm 100\%$ efficiency, respectively, indicating the CMJ in S1 and S2 states can behave as perfect spin-filters. Figure 3(b) plots the SR as a function of ΔT for the CMJ in S1/S3 and S2/S4 states. It can be seen that both the two cases exhibit good switching performance with the SRs up to $10^4\%$, indicating the CMJ can behave as a good molecular switch when it converts between S1 and S3 (S2 and S4) states upon photo-excitation.

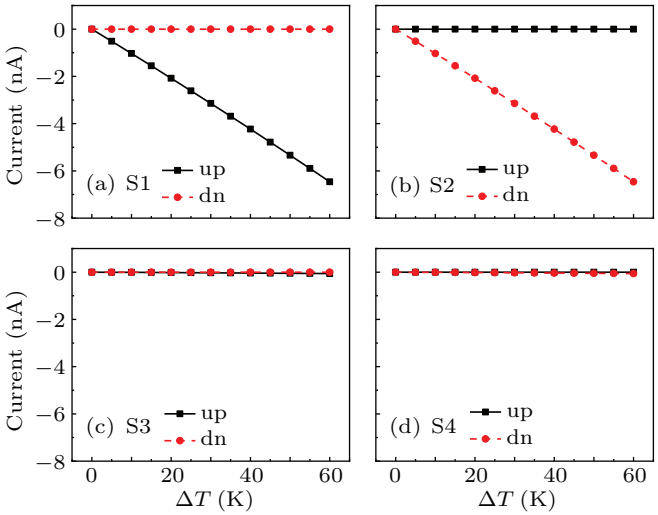


Fig. 2. Calculated thermally-driven spin-dependent currents as a function of ΔT with $T_{\rm L} = 300$ K for the CMJ in (a) S1, (b) S2, (c) S3 and (d) S4 states, respectively.

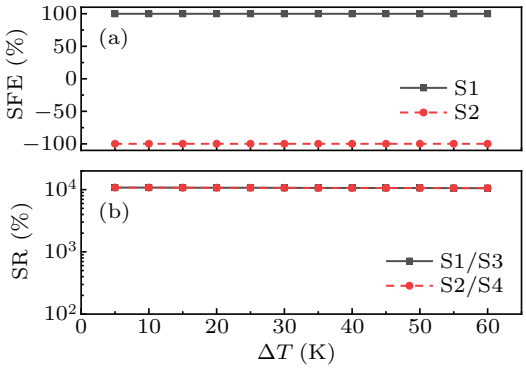


Fig. 3. (a) Calculated spin filtering efficiency (SFE) as a function of ΔT for the CMJ in S1 and S2 states. (b) Calculated switching ratio (SR) as a function of ΔT for the CMJ in S1/S3 and S2/S4 states.

Based on Eq. (1), we know that the thermally-driven spin-dependent currents are essentially determined by the product of two factors, namely, $T_\sigma(E)$ and the difference between the Fermi–Dirac distribution function of two electrodes, i.e., $(f_{\rm L} - f_{\rm R})$. Figure 4(a) plots the $f_{\rm L}$ and $f_{\rm R}$ with different temperature ($T_{\rm L} = 300$ K and $T_{\rm R} = 240$ K) as a function of $(E - E_{\rm F})$, respectively. Here, the $E_{\rm F}$ is the Fermi energy. It can be seen clearly that the carrier (hole when $E < E_{\rm F}$ and electron when $E > E_{\rm F}$) concentration in the hot LE is always higher than that in the cold RE. Therefore, both the holes and electrons flow from the hot LE to the cold RE. And thus the former results in a positive current $I_{\rm h}$, while the latter leads to a negative current $I_{\rm e}$ due to the holes are positively charged and the electrons are negatively charged. Moreover, as shown in

the insert of Fig. 4(a), $(f_L - f_R)$ is a strictly symmetric function with respect to E_F, and also presents a typical exponential decaying feature. This indicates that only $T_\sigma(E)$ in the energy region near E_F contributes to the thermally-driven currents, while the contribution from $T_\sigma(E)$ in other energy regions can be actually ignored. Meantime, in order to avoid the cancelation between the positive I_h and negative I_e and obtain observable thermally-driven currents, $T_\sigma(E)$ in the energy region near E_F should be anti-symmetric about E_F. Taking S1 and S3 states as examples, in Fig. 4(b), we plot their spin-resolved transmission spectra. Clearly, an obvious and a very faint spin-up transmission peak just above the E_F appears in S1 and S3 states, respectively, while we cannot observe any spin-down transmission peak near E_F. Those distinct transmission characteristics can be elucidated by the spatial distribution of molecular projected self-consistent Hamiltonian (MPSH) orbitals[33] around E_F. As shown in Fig. 4(b), there is only one spin-up MPSH orbital (185) just above E_F at 0.018 eV and 0.026 eV for S1 and S3 states, respectively. As shown by the spatial distribution in the insert of Fig. 4(b), the spin-up MPSH 185 is a relatively extended and completely localized orbital in S1 and S3 sates, respectively. As further shown by the spin-resolved projected density of states (PDOS) in Fig. S1(a) in the supporting information, for S1 state, there is a strong spin-up PDOS from the PFCF molecule, a weak spin-up PDOS from the SWACNT bridge and an observable spin-up PDOS from the DDP molecule at 0.018 eV. Hybrid between them leads to the relatively extended spin-up MPSH 185 orbital and the obvious spin-up transmission peak in S1 state at corresponding energy region. As shown by the spin-resolved projected density of states (PDOS) in Fig. S1(b) in the supporting information, for S3 state, there is still a strong spin-up PDOS from the PFCF molecule, a weak spin-up PDOS from the SWACNT bridge at 0.026 eV, but the spin-up PDOS from the CPD molecule vanishes, resulting in the completely localized spin-up MPSH 185 orbital and the very faint transmission peak in S3 state at corresponding energy region. In stark contrast, no any spin-down MPSH orbital can be found near E_F in two states (see Figs. S1(a) and S1(b) in the supporting information, no any spin-down PDOS hybrid near E_F), bringing out the disappearance of spin-down transmission peak in the vicinity of E_F. Figures 4(c) and 4(d) then plot the spin-resolved current spectra, $J_\sigma(E) = T_\sigma(E) \times (f_L - f_R)$, as a function of $(E - E_F)$ for S1 and S3 states with $\Delta T = 60$ K. Clearly, the size of the integral area of $J_\sigma(E)$ below and above the E_F determines the magnitude of the positive I_h and negative I_e, respectively. In S1 state, as shown in Fig. 4(c), one can observe an obvious J_{up} peak just above and below E_F, respectively. The integral area of J_{up} peak above E_F is much larger than that below E_F. As a result, the negative spin-up I_e overruns the positive spin-up I_h, giving rise to an obvious nonzero net negative I_{up}. Meantime, no any J_{dn} peak can be found due to the disappearance of spin-down transmission peak near E_F, resulting in the vanishing of I_{dn}. In S3 state, as shown in Fig. 4(d), there is no any J_{dn} peak around E_F, meanwhile the J_{up} peak around E_F is also reduced significantly. Therefore, both I_{up} and I_{dn} are strongly suppressed in S3 state.

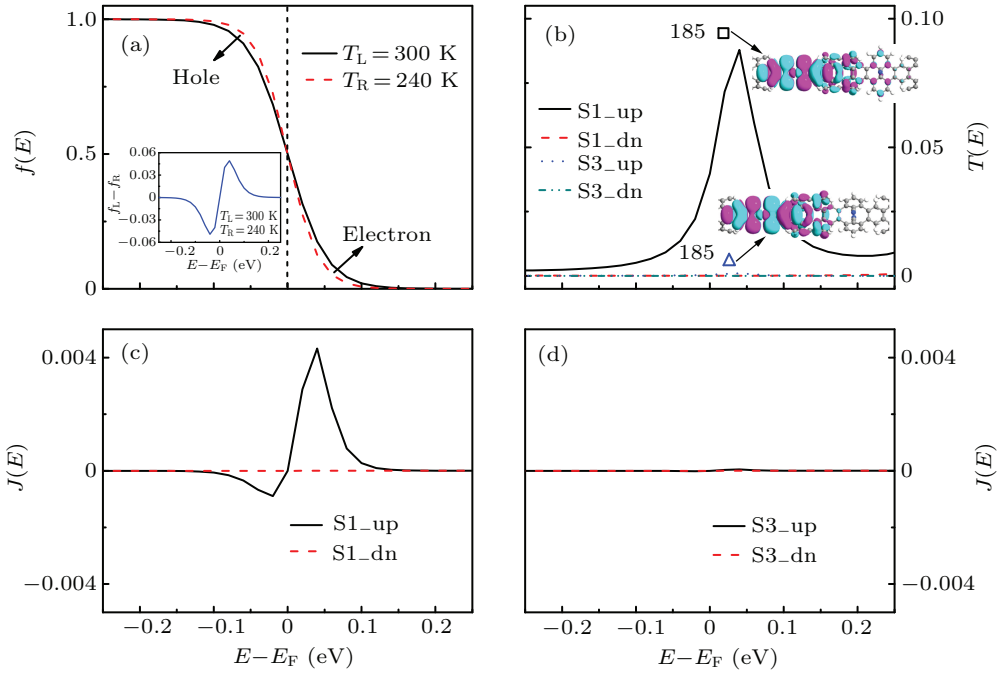


Fig. 4. (a) Calculated Fermi–Dirac distribution function of electrons in LE with $T_L = 300$ K and in RE with $T_R = 240$ K. The insert presents the difference between them. (b) Calculated spin-resolved transmission spectra for S1 and S3 states. The positions of molecular projected self-consistent Hamiltonian (MPSH) eigenvalues are marked with squares for S1 state and with triangle for S3 state, respectively. The inserts show the spatial distributions of corresponding MPSH orbitals. (c) Calculated spin-resolved current spectra for S1 state with $\Delta T = 60$ K. (d) Calculated spin-resolved current spectra for S3 state.

3.2. Thermal spin molecular AND, OR and NOT gates

Based on these thermally-driven spin-dependent transport properties of the PFCF+DDP/CPD-based CMJ, we can design three elementary thermal spin molecular logic gates, taking the magnetic field in different directions and the light with different wavelengths as input signals and the produced spin-polarized current or total current as output signal. Those thermal spin molecular gates utilize two different types of external stimuli as input signals, and then avoid the problem of modulating the direction of the external magnetic field on a very small scale.

3.2.1. The design of AND gate

As shown in Fig. 5(a), the magnetic field and light are the input signals A and B, respectively, and the produced I_{up} is the output signal Y. For A and B, the upward/downward magnetic field and the UV/VIS light are defined as logic 1/0, respectively. For Y, the high/low I_{up} is taken as logic 1/0. As one can see from Figs. 2(a)–2(d), the I_{up} is only high in S1 state, and it is extremely low in S2, S3 and S4 states. Clearly, the CMJ only produces logic 1 ($Y = 1$) when the magnetic field is up ($A = 1$) and the light is UV ($B = 1$), namely, Y is the logical product of A and B (see the truth table in Fig. 5(a)), indicating the AND logical relationship is established.

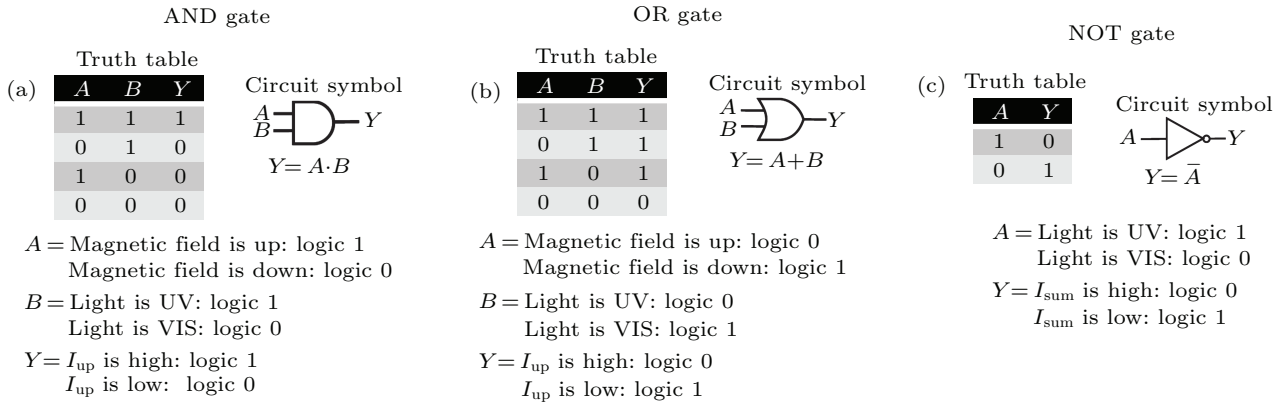


Fig. 5. The inputs, output, truth table and circuit symbol for thermal spin molecular logic (a) AND, (b) OR and (c) NOT gates.

3.2.2. The design of OR gate

As opposed to the AND gate, for A and B in the OR gate, the downward/upward magnetic field and the VIS/UV light are defined as logic 1/0, respectively. For Y, the low/high I_{up} is taken as logic 1/0. It can been seen from Figs. 2(a)–2(d) that the I_{up} is only high in S1 state, and it is extremely low in S2, S3 and S4 states. Clearly, the CMJ only produces logic 0 ($Y = 0$) when the magnetic field is up ($A = 0$) and the light is UV ($B = 0$), otherwise it produces logic 1 ($Y = 1$) when the magnetic field is down ($A = 1$) or the light is VIS ($B = 1$). That is to say that Y is the logical sum of A and B (see the truth table in Fig. 5(b)), and thus the OR logical function is achieved.

3.2.3. The design of NOT gate

The magnetic field is always up. The input signal A and the output signal Y correspond to the light and the produced total current I_{sum}, respectively. For A, the UV/VIS light is defined as logic 1/0. For Y, the high/low I_{sum} is defined as logic 0/1. From Figs. 2(a) and 2(c), it can be seen that the I_{sum} is high and extremely low in S1 (i.e., $Y = 0, A = 1$) and S3 (i.e., $Y = 1, A = 0$) states, respectively. Clearly, Y is the logic inversion of A (see the truth table in Fig. 5(b)), indicating the NOT logical operation is realized.

4. Conclusion

We have studied theoretically the thermally-driven spin-dependent transport properties of the PFCF+DDP/CPD-based combinational molecular junction consisting of a PFCF molecule and a DDP/CPD molecule with SWACNT bridge and electrodes by using the DFT+NEGF methodology. The results demonstrate that the magnetic field and light can effectively regulate the thermally-driven spin-dependent currents. Perfect thermal spin-filtering effect and good thermal switching effect are achieved. The results are analyzed from four aspects, i.e., the Fermi–Dirac distribution function, the spin-resolved transmission spectra, the spatial distribution of MPSH orbitals, and the spin-resolved current spectra. On the basis of these intriguing thermally-driven spin-dependent transport properties, we have designed three elementary thermal spin molecular AND, OR and NOT gates. To summarize, our studies provide a route to realize thermal spin molecular logic gates avoiding the problem of modulating the direction of the external magnetic field on a very small scale by constructing the combinational molecular junction, which may have a great development prospect in the fields of spin caloritronics and digital electronics.

Acknowledgements

Project supported by the Natural Science Foundation of Shandong Province, China (Grant No. ZR2021MA059) and the Major Scientific and Technological Innovation Project (MSTIP) of Shandong Province, China (Grant No. 2019JZZY010209).

References

[1] Wolf S A, Awschalom D D, Buhrman R A, Daughton J A, von Molnár S, Roukes M L, Chtchelkanova A Y and Treger D M 2001 *Science* **294** 1488
[2] Lakshmi S, Roche S and Cuniberti G 2009 *Phys. Rev. B* **80** 193404
[3] Li B, Zhu L, Wu C, Yao K and Chang C R 2020 *Nanotechnology* **31** 145206
[4] Wang Z Q, Tang F, Dong M M, Wang M L, Hu G C, Leng J C, Wang C K and Zhang G P 2020 *Chin. Phys. B* **29** 067202
[5] Zeng M, Shen L, Su H, Zhang C and Feng Y 2011 *Appl. Phys. Lett.* **98** 092110
[6] Zeng M, Shen L, Zhou M, Zhang C and Feng Y 2011 *Phys. Rev. B* **83** 115427
[7] Kang J, Wu F and Li J 2012 *Appl. Phys. Lett.* **100** 233122
[8] Zou D, Zhao W and Yang C 2019 *Org. Electron.* **69** 120
[9] Zhao P and Chen G 2020 *J. Magn. Magn. Mater.* **493** 165712
[10] He H B and Zhao P 2020 *Phys. E* **121** 114130
[11] Mitchell R H 1999 *Eur. J. Org. Chem.* **1999** 2695
[12] Williams R V, Edwards W D, Mitchell R H and Robinson S G 2005 *J. Am. Chem. Soc.* **127** 16207
[13] Zhao P, Fang C F, Xia C J, Liu D S and Xie S J 2008 *Chem. Phys. Lett.* **453** 62
[14] Uchida K, Takahashi S, Harii K, Ieda J, Koshibae W, Ando K, Maekawa S and Saitoh E 2008 *Nature* **455** 778
[15] Bauer G E W, Saitoh E and van Wees B J 2012 *Nat. Mater.* **11** 391
[16] Boona S R, Myers R C and Heremans J P 2014 *Energ. Environ. Sci.* **7** 885
[17] Taylor J, Guo H and Wang J 2001 *Phys. Rev. B* **63** 121104
[18] Taylor J, Guo H and Wang J 2001 *Phys. Rev. B* **63** 245407
[19] Brandbyge M, Mozos J L, Ordejón P, Taylor J and Stokbro K 2002 *Phys. Rev. B* **65** 165401
[20] Soler J M, Artacho E, Gale J D, García A, Junquera J, Ordejón P and Sánchez-Portal D 2002 *J. Phys.: Condens. Matter* **14** 2745
[21] Fu H H, Wu D D, Zhang Z Q and Gu L 2015 *Sci. Rep.* **5** 10547
[22] Zhu L, Li R and Yao K 2017 *Phys. Chem. Chem. Phys.* **19** 4085
[23] Zhu L, Zou F, Gao G and Yao K 2017 *Sci. Rep.* **7** 497
[24] Zhu L, Li B and Yao K 2018 *Nanotechnology* **29** 325206
[25] Zhu L, Li B, Ma H, Qian M and Yao K 2019 *Nanotechnology* **30** 445204
[26] Perdew J P, Burke K and Ernzerhof M 1996 *Phys. Rev. Lett.* **77** 3865
[27] Troullier N and Martins J 1991 *Phys. Rev. B* **43** 1993
[28] Monkhorst H J and Pack J D 1976 *Phys. Rev. B* **13** 5188
[29] Büttiker M, Imry Y, Landauer R and Pinhas S 1985 *Phys. Rev. B* **31** 6207
[30] Zhang C, Du M H, Cheng H P, Zhang X G, Roitberg A E and Krause J L 2004 *Phys. Rev. Lett.* **92** 158301
[31] Valle M D, Gutiérrez R, Tejedor C and Cuniberti G 2007 *Nat. Nanotech.* **2** 176
[32] Motta C, Trioni M I, Brivio G P and Sebastian K L 2011 *Phys. Rev. B* **84** 113408
[33] Stokbro K, Taylor J, Brandbyge M, Mozos J L and Ordejón P 2003 *Comput. Mater. Sci.* **27** 151